Applied Thermal Engineering 236 (2024) 121666

Contents lists available at ScienceDirect

Applied Thermal Engineering

journal homepage: www.elsevier.com/locate/apthermeng

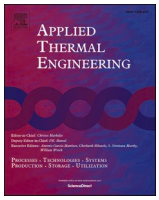

Research Paper

Membrane-based packed-sheet liquid desiccant dehumidification system

Amin M. Elsafi, Majid Bahrami *

Laboratory for Alternative Energy Conversion (LAEC), School of Mechatronic Systems Engineering Simon Fraser University, Surrey, BC V3T 0A3, Canada

ARTICLE INFO

Keywords:
Liquid desiccant
Dehumidification
Packed-Sheet
Membrane

ABSTRACT

Humidity control plays a vital role in both buildings and greenhouses. The thermally-driven liquid desiccant dehumidification systems are getting an increasing traction because of their high moisture removal capacity and the possibility of their integration with waste-heat or renewable energy sources. In this work, a novel design concept for liquid desiccant dehumidification systems is proposed to overcome the practical challenges of the conventional systems, such as solution carryover, crystallization, and corrosion. The presented system utilizes a compact "packed-sheet" sorption bed that houses spherical membrane-based micro-absorbers with LiBr as a liquid desiccant. A bench-scale system is designed and tested under the typical dehumidification working conditions. The experimental results showed that the proposed design has up to two-fold higher moisture removal rate per volume (MRR = 75 g/s-m^3) than a conventional LiBr liquid desiccant dehumidification system (MRR = 35 g/s-m^3). In addition, a one-dimensional coupled heat and mass transfer mathematical model is developed to simulate the transient behavior of the proposed system. An optimization study, using the validated model, suggested that the performance of proposed design can be maximized to realize moisture removal rates of up to 135 g/s-m^3 (270% higher than the conventional liquid desiccant systems) with a coefficient of performance of 0.25.

1. Introduction

The building sector (residential and commercial) is the largest energy consumer, consisting of approximately 40% of the global energy consumption as of 2019 [1]. The required energy to control the temperature and humidity for human comfort is estimated as 50% of the building's total energy consumption [2]. Several serious health problems which are caused by mildew, viruses, reduction of air quality, and the occupants' discomfort in buildings are all associated with excessive humidity [3]. Humidity control also plays a vital role in greenhouse food production. Low humidity leads to reduced stem lengths and leaf sizes [4], while excessive humidity along with condensation can lead to fungal diseases, leaf necrosis, and soft and thin leaves.

Air dehumidification can be achieved using heat pumps (cooling-condensation), membrane-based heat/enthalpy exchangers, and sorption (solid or liquid desiccant) desiccant dehumidification systems among other technologies. Despite their high efficiency, using heat pumps for dehumidification comes with challenges, such as high initial and operating costs, maintenance issues, ozone depletion potential, and global warming potential. On the other hand, membrane-based heat/enthalpy exchangers are simple, inexpensive, and have an overall efficiency of 60–90% [5,6], but they are prone to frost formation in cold climates and are less effective during the summer periods [7]. The thermally-driven sorption dehumidification systems are getting an increasing traction because they can help alleviating the burden on the electricity generation sector, and can significantly reduce the emissions associated with ventilation and air conditioning systems, especially, when they are integrated with a waste-heat or renewable energy source. As far as large applications are concerned (ex: buildings and greenhouses), liquid desiccant dehumidification systems are more favorable than solid desiccant systems because of their higher sorption capacity [8,9]. Another advantage of using an inorganic salt solution in liquid desiccant dehumidification systems is that it can improve the indoor air quality as these salts act as disinfectants [10].

Nevertheless, the research on liquid desiccant dehumidification systems is still limited to numerical simulations or laboratory-scale experiments rather than practical applications [10]. The conventional liquid desiccant dehumidification systems have a major practical problem which is the risk of solution carryover by the forced sorbate stream [2,11]. Another key issue in working with liquid desiccant systems is the crystallization of the salt solution which can block the piping network and damage the pumping system. The corrosive nature of the inorganic salt solutions also presents a limitation on the material that can be used

* Corresponding author.
E-mail addresses: aelsafi@sfu.ca (A.M. Elsafi), mbahrami@sfu.ca (M. Bahrami).

https://doi.org/10.1016/j.applthermaleng.2023.121666
Received 27 June 2023; Received in revised form 10 September 2023; Accepted 22 September 2023
Available online 22 September 2023

Nomenclature

Abbreviations

MRR	moisture removal rate, g/s-m^3
DCOP	dehumidification coefficient of performance, -

Roman Symbols

A_{cs}	cross-sectional area, m^2
c_P	specific heat capacity, J/kg-K
d_{caps}	diameter of the microcapsules, m
D_{wv}	water vapor mass diffusivity, m^2/s
h_c	convective heat transfer coefficient, W/m^2-K
h_m	convective mass transfer coefficient, m/s
h_{fg}	enthalpy of vaporization, kJ/kg
H	channel height, m
ΔH_s	heat of absorption, kJ/kg
k	thermal conductivity, W/m-K
L	sorption bed length, m
Le	Lewis number, -
Nu	Nusselt number, -
P	pressure, kPa
Pr	Prandtl number, -
U_h	overall heat transfer coefficient, W/m^2-s
U_m	overall mass transfer coefficient, m/s
Re	Reynolds number, -
RH	relative humidity, -
t	thickness, m
t_{deh}	dehumidification process (i.e., half-cycle) time, sec
T	temperature, ^{o}C
u	air velocity, m/s
X	sorbent water uptake, g_w/g_{dry}

Greek symbols

ε	void fraction, -
ρ	density, kg/m^3
ω	humidity ratio, g_w/g_{air}

Subscripts

a	related to air
s	related to sorbent
pro	related to process air
a	related to regeneration air
∞	related to ambient fluid

to construct the dehumidifier.

Comprehensive literature reviews on liquid desiccant dehumidification systems were presented by [2,10,12]. The absorber is the most critical component of the liquid desiccant systems, and has a significant impact on their size, cost, and efficiency. Although there are different absorber designs proposed in the literature, the ones that are used for dehumidification systems are the packed-column and membrane absorbers. A comparison between these two absorber designs is presented in Table 1. One can conclude that packed-column absorbers offer more compact designs than membrane absorbers as they tend to have higher moisture removal rates per volume (MRR, g/s-m^3). Also, the packed-column absorber is considered to be the most practical and mature design that can be used for dehumidification systems because of its simplicity and scalability. The packed-column absorber works in the falling-film mode in which the humid air is brought into direct contact with a concentrated salt solution to absorb the moisture. The main mechanism for the mass transfer in this type of absorbers is the diffusion through the liquid solution film, which is a rather slow process and presents a fundamental limitation on maximum absorption rates (and realization of compact designs). The major concern in using packed-column absorbers in dehumidification applications is the risk of solution carryover by the forced air stream [2,11]. Packed-column absorbers require high solution flow rates to achieve good wetting in order to avoid the decrease in efficiency due to the reduction in the reaction surface-to-volume ratio [13]. High flow rates increase the risk of solution carryover which can cause respiratory problems for the occupants.

In this work, a novel design concept for absorbers is proposed that can be used in dehumidification systems. The proposed absorber provides compactness (i.e., high surface area per volume), permits working in the crystallization region, and eliminates the metal corrosion associated with the corrosive hygroscopic salts. This is achieved by creating spherical micro-absorbers by encapsulating an aqueous hygroscopic salt (like LiBr, LiCl, or $CaCl_2$) solution inside an elastic semi-permeable membrane shell. The shell is highly permeable to sorbate but impermeable to the salt and its solution. Due to the indirect contact between the liquid desiccant and the air, problems such as solution carryover and corrosion can be completely eliminated.

Table 1
A summary of liquid desiccant absorbers used in dehumidification systems.

Reference	Absorber Design	Liquid Desiccant	Specific Area [m^2/m^3]	Inlet air temperature [^{o}C]	Inlet air humidity [g/kg]	Moisture removal rate, MRR [g/s-m^3]
[14]		LiBr	396	25.4–35.4	9.5–18.2	23.7–35
[14]	Packed-column absorber	LiCl	396	26.9–35.1	9.8–20.4	20.9–48.95
[15]		LiCl	450	25–30	10.8–16.2	–
[11]		$CaCl_2$	608	30	18.873	–
[16]		LiBr	–	23.6–35.4	10.4–18.7	–
[17]		LiCl	210	30	18	7.6–17
[18]		LiBr	–	–	–	–
[19]		LiBr	–	23.6–35.7	11.2–22.8	–
[20]		LiCl	550	35	15	6.2–16
[21]		$CaCl_2$	390	31	18	8–24.2
[22]		$CaCl_2$	608	26.8–39.0	16–24	–
[23]		LiCl	–	26–31	10.5–17.9	–
[24]	Membrane absorber	LiBr	–	30	19	–
[25]		LiBr	–	35	19.4	–
[26]		LiBr	–	30	18	8.5–8.7
[27]		LiBr	–	35	17.8–25.26	2.5–5.6

2. Experimental setup

2.1. System description

The core of the system is the spherical micro-absorbers (microcapsules) that permit heat and mass transfer between an encapsulated liquid desiccant and the humid air through a semi-permeable membrane. The working principles of the spherical micro-absorbers during absorption (dehumidification) and regeneration processes is illustrated in Fig. 1. During the dehumidification (absorption) process, the water vapor diffuses through the membrane and is absorbed by the encapsulated liquid desiccant. During the regeneration process, heat is transferred to the microcapsules to release the absorbed moisture from the liquid desiccant.

The microcapsules were produced using a microfluidic technique. Briefly, a custom-built microfluidic device was used to create a double emulsion in order to encapsulate the aqueous liquid sorbent solutions (water-phase) inside a UV curable resin (oil-phase) that acts as the shell and becomes solid when exposed to a UV light source. The liquid sorbent used in the presented experiment was LiBr aqueous solution, and the UV curable resin used to make the shell was TEGO Rad 2650 (donated by Evonik Industries, USA). The formed spherical microcapsules are highly uniform in size and can be designed to have a micro-scale size (500–1,000 μm diameter) and provide surface-to-volume ratios between 6,000–12,000 m^2/m^3, which is up to two orders of magnitude higher than the conventional packed-column absorbers (200–600 m^2/m^3 [14,21,28–31]). A microscopic image of a micro-capsule that contains the aqueous LiBr solution is shown in Fig. 2**a**. The capsule was heated to remove some of the water from the solution, and that resulted in the formation of the salt crystals as shown in Fig. 2**b**. This confirms that micro-capsules can tolerate salt crystallization and has the potential to eliminate the solution carryover and corrosion issues because the solution/salt will be contained inside the membrane.

A prototype was built based on the "packed-sheet" design in which about 8 g of microcapsules were used. The sheet-type sorption bed was comprised of two parallel stainless steel mesh layers, Fig. 3**a**, one at the bottom and the other at the top, supported by a 3D printed frame (ABS plastic) with dimensions of 180 mm × 30 mm × 2 mm, see Fig. 3**b** and Fig. 3**c**. The 425 μm nominal aperture of the stainless-steel mesh allowed the microcapsules, with a 700 μm outer diameter, to be accommodated and kept between the mesh layers without using any binder, see Fig. 3**d**. The voids in the mesh layers enabled direct contact between the microcapsules and air streams, which would result in a better heat and mass transfer, thus better dehumidification performance, due to the direct air flow around the microcapsules. Two 3D printed (acrylate-like material) parts, top and bottom parts in Fig. 4, were used to house the packed-sheet, to provide an inlet and outlet for the air streams, and as a means to install the temperature, relative humidity, and pressure transducer sensors. The final assembly of the packed-sheet absorber is shown in Fig. 5. A 12 mm thick rubber insulation was used to minimize the heat loss from the bed.

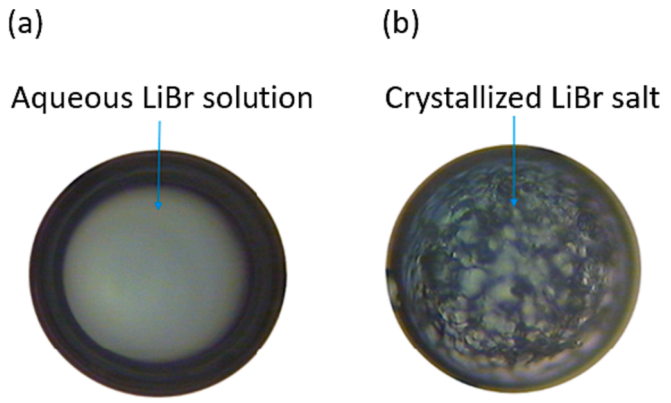

Fig. 2. Microscopic images of a micro-capsule that contains (a) LiBr solution and (b) crystallized LiBr inside the spherical membrane.

The working principle of the proposed dehumidification system is illustrated in Fig. 6. The process air stream represents the incoming air that should be dehumidified. During the dehumidification process, the process air is passed through the sorption bed (packed sheet) for the moisture to be absorbed by the liquid desiccant inside the microcapsules. During the regeneration process, the incoming air is heated to 60–80 °C to decrease the relative humidity of the air and make it dry to enable the moisture transfer from the microcapsules to the air (regenerating the microcapsules).

As shown in Fig. 7, the experimental setup consists of a compressed air supply, two environmental champers (C1 and C2), two three-way valves (V1 and V2), and a sorption bed. Two environmental champers (Cellkraft, P-10C) were used to control the temperature and humidity of the supplied air during the dehumidification and regeneration cycles. Three-way vales were used to direct the air flow, alternatively to the sorption bed and the exhaust line. The test bed was equipped with two relative humidity sensors (Vaisala HUMICAP® HMP110) and two T-type thermocouples (Omega Eng. Inc, Canada) installed at the inlet and outlet of the sorption bed to measure the relative humidity and temperature of the inlet and outlet air. The flow rate of the air supplied to the sorption bed was measured using a flow meter (ALICAT, M−50SLPM−D/SM). A differential pressure transducer (Model 267, Setra Systems, Inc.) was used to measure the pressure drop across the bed.

2.2. Test procedure

With reference to Fig. 7, the following procedure was followed to perform the tests:

1. Before passing the air through the sorption bed, compressed air was directed through the environmental chambers (C1 and C2) to the control the temperature and relative humidity of the air and set them at the desired working conditions to mimic typical conditions during dehumidification and regeneration processes. Both control valves (V1

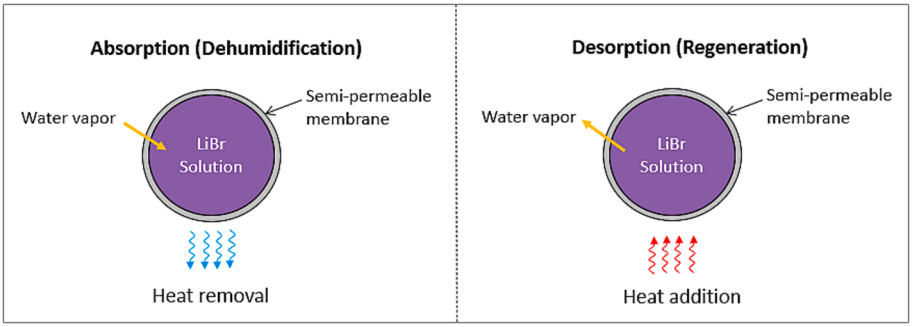

Fig. 1. Absorption and regeneration principles of the proposed spherical micro-absorbers for dehumidification applications.

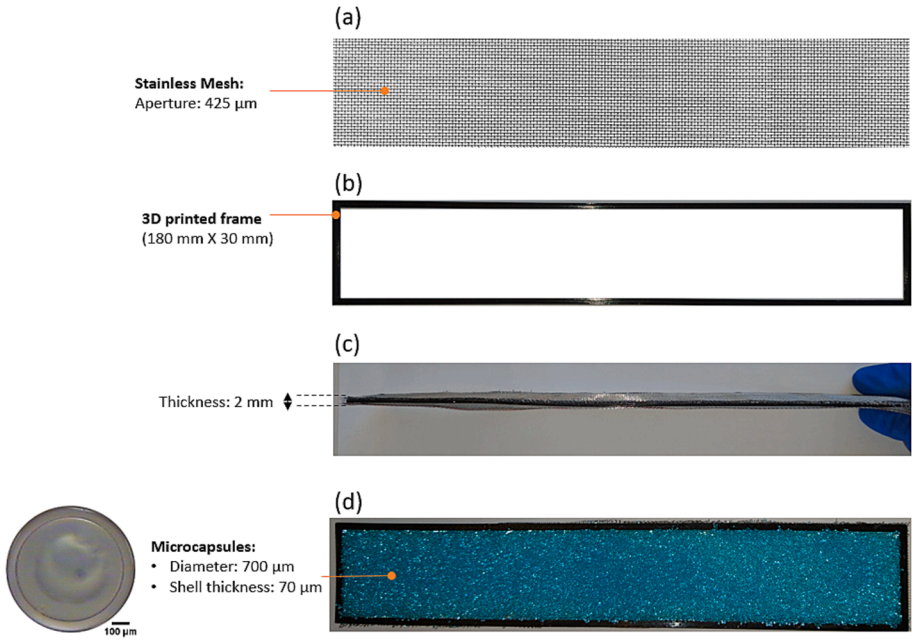

Fig. 3. The components of a single packed-sheet: (a) stainless mesh, (b) 3D printed frame, (c) meshes attached to the frame before packing, and (d) packed microcapsules.

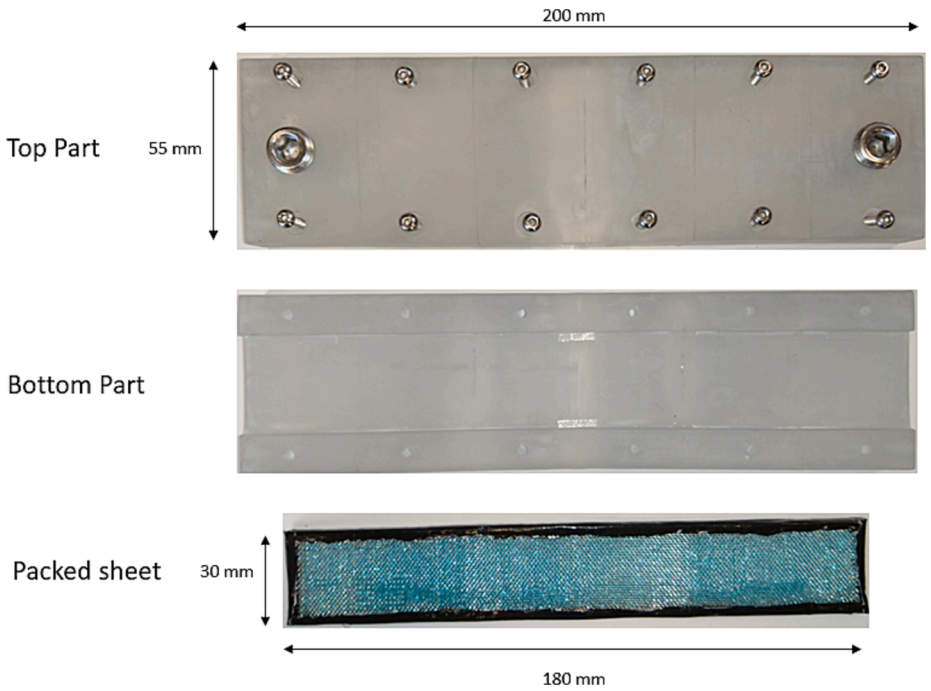

Fig. 4. The components of the sorption bed (before assembly).

and V2) were connected to the exhaust lines during this step until the systems stabilized and the required working conditions were achieved. Table 2 shows the operating conditions of the process and regeneration air during the conducted tests.

2. During the regeneration process, the three-way control valve (V1) was closed (connected to the exhaust line), and the other valve (V2) was opened to direct the hot and dry air (supplied from the environmental chamber C2). With the passage of time, the absorbed water was removed from the sorption bed and the microcapsules became regenerated. Once the required regeneration half-cycle time was achieved, the three-way vale (V2) was used to discharge the hot regeneration air to the surrounding environment through the exhaust line.

3. During the dehumidification process, the control valve (V1) was opened to allow the humid "process" air (supplied from the environmental chamber C1) to follow through the sorption bed. After the required half-cycle dehumidification time had passed, the process air was bypassed to the exhaust line connected to the surrounding environment by switching V1 to the other direction.

4 In order to prepare the sorption bed for the next dehumidification process, Step 1 was repeated to start the regeneration process.

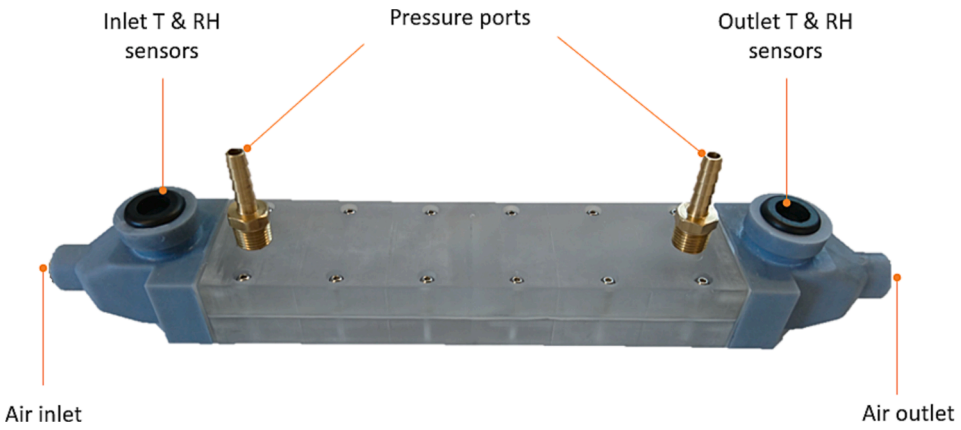

Fig. 5. The prototype of the sorption bed.

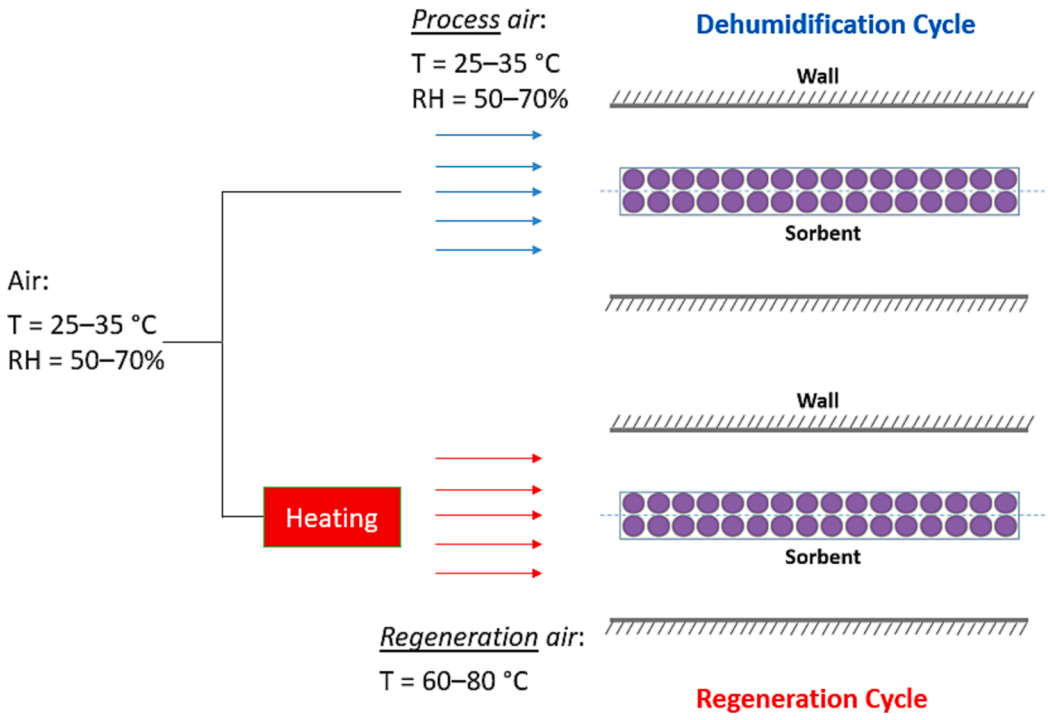

Fig. 6. An illustration of the working principle of the proposed dehumidification system.

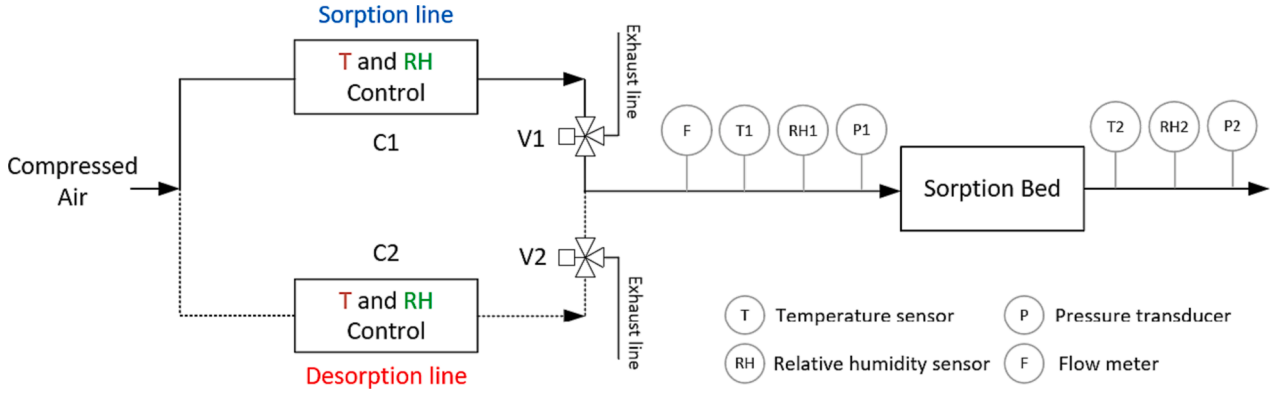

Fig. 7. A schematic of the custom-built experimental setup.

Table 2
The operating conditions for the dehumidification system.

	Temperature [°C]	Relative humidity [%]	Humidity ratio [g/kg]	Half-cycle time [min]	Flow rate [LPM]
Process air	25–35	50–70	8–15	30	3–10
Regeneration air	60–70	3–7	10–15	30	3–10

2.3. Key performance indicators

The key performance indicator (KPI) that was used to measure the performance of the proposed dehumidification system is the moisture removal rate (MRR, g/s-m^3), defined as:

$$MRR = \frac{\text{Rate of moisture removal}}{\text{Volume}} = \frac{\left[\int_0^{t_{deh}} \dot{m}_{pro}\left(\omega_{pro,i} - \omega_{pro,o}\right)\cdot dt\right] \Big/ t_{deh}}{\text{Volume}} \quad (1)$$

where $\dot{m}_{pro}$ is the mass flow rate, $\omega_{pro,i}$ and $\omega_{pro,o}$ are the inlet humidity and the outlet humidity of the process air, respectively. The parameter t_{deh} is the time taken during dehumidification process (half-cycle time). The volume considered in Eq. (1) is the internal volume of the sorption bed. Typical values for moisture removal rates for the state-of-the-art packed-column absorbers that use LiBr hygroscopic salt are within the 20–35 g/s-m^3 range.

Another performance indicator, the dehumidification coefficient of performance (*DCOP*,-), was used to measure the power consumed to achieve the required moisture removal rate (i.e., the ratio between the removed latent heat to energy input). Mathematically, the coefficient of performance is expressed as:

$$DCOP = \frac{\text{Latent heat removed}}{\text{Energy input}} = \frac{\int_0^{t_{deh}} \dot{m}_{pro} h_{fg}\left(\omega_{pro,i} - \omega_{pro,o}\right)\cdot dt}{\int_0^{t_{reg}} \dot{m}_{reg} c_p\left(\Delta T_{reg}\right)\cdot dt} \quad (2)$$

where, c_p is the specific heat of the air, and ΔT_{reg} represents the difference between the air inlet and outlet temperature during the heating of the regeneration air, the fan energy to overcome the pressure drop in the packed-sheet absorber is negligible compared to the air heater.

2.4. Uncertainty analysis

The method proposed by Kline and McClintock [32] was used to compute the uncertainty of the present experimental data as follows:

$$Y = f(X_1, X_2, X_3, \ldots)$$

$$\partial Y = \sqrt{\left(\frac{\partial Y}{\partial X_1}\delta X_1\right)^2 + \left(\frac{\partial Y}{\partial X_2}\delta X_2\right)^2 + \left(\frac{\partial Y}{\partial X_3}\delta X_3\right)^2 + \ldots} \quad (3)$$

where ∂Y gives the overall uncertainty associated with parameter Y, and $\partial X_{1,2,3,\ldots}$ are the uncertainties associated with measured parameters $X_{1,2,3,\ldots}$. The uncertainty of the used devices used in the experiments are listed in Table 3.

The analysis showed that the moisture removal rate (MRR) can be calculated with ±4.5% uncertainty, while the uncertainty in calculating the dehumidification coefficient of performance (DCOP) is ± 5%.

3. Mathematical modeling

A schematic for the proposed packed-sheet sorption bed is presented in Fig. 8**a**. The process/regeneration air is passed through the channel and is exposed to a packed-sheet filled with microcapsules that contain a LiBr liquid desiccant. The heat and mass transfer paths across the microcapsules is illustrated in Fig. 8**b**. The main assumptions used to develop the mathematical model are [33–35]:

- 1-D flow in the Z-direction;
- Incompressible fully-developed laminar flow;
- Negligible heat conduction and mass diffusion along the length;
- Constant thermo-physical properties of the sorbent;
- The air flows past the spherical micro-absorbers with a constant area-averaged effective velocity; and.
- The Lewis number, *Le*, which reflects the ratio of the convective heat transfer coefficient to the convective mass transfer coefficient is equal to the unity for air [13].

Table 3
The uncertainty of the devices used in the experiments.

Parameter	Instrument	Range	Accuracy
Humidity	Vaisala HUMICAP® HMP110	0–100 % RH	± 1.5% RH for 0…+40 °C ± 3.0% RH for −40 …0 °C
Temperature	Omega, T type thermocouple	0–200 °C	± 0.5 °C
Flow rate	ALICAT, M-50SLPM-D/SM	0–10 *lpm*	0.2%
Differential Pressure Transducer	Setra Model 267	0–5″ *W.C.* (0–1244 *Pa*)	± 0.0125″ *W.C.* (±3 *Pa*)

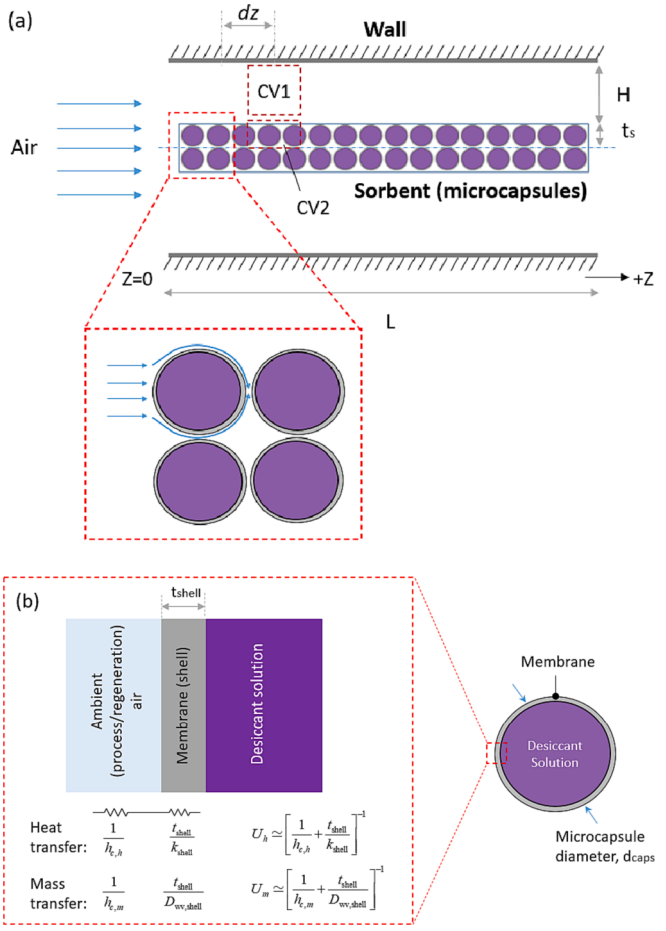

Fig. 8. (a) A schematic of the packed-sheet sorption bed with encapsulated liquid sorption; and (b) heat and mass transfer across the microcapsules (i.e., micro-absorbers).

The mass continuity and energy balance equations were applied to infinitesimal control volumes (with a dz length) in the air (CV1) and sorbent (CV2) domains, and are expressed as follows:

Air (CV1):

Mass Balance:

$$\frac{\partial \omega_a}{\partial t} = -u_a \frac{\partial \omega_a}{\partial z} - \frac{\rho_s A_{cs,s}}{\rho_a A_{cs,a}}(1-\varepsilon)\frac{\partial X_s}{\partial t} \tag{4}$$

Energy Balance:

$$\frac{\partial T_a}{\partial t} = -u_a \frac{\partial T_a}{\partial z} - \frac{6U_h}{\rho_a d_{\text{caps}} c_{p,a}} \frac{A_{cs,s}}{A_{cs,a}}(1-\varepsilon)(T_a - T_s) \tag{5}$$

Sorbent (CV2):

Mass Balance:

$$\frac{\partial X_s}{\partial t} = \frac{6U_m}{\rho_s d_{\text{caps}}}(\omega_a - \omega_s) \tag{6}$$

Energy Balance:

$$\frac{\partial T_s}{\partial t} = \frac{\Delta H_s}{c_{p,s}} \frac{\partial X_s}{\partial t} + \frac{6U_h}{\rho_s c_{p,s} d_{\text{caps}}}(T_a - T_s) \tag{7}$$

In the above equations, ω, T, refer X to the humidity and temperature, and water uptake, respectively. The subscripts a and s are related to the air and sorbent, respectively. The parameter u_a denotes the air velocity.

The active volume of the sorbent in the packed volume can be estimated by:

$$V_s = (1-\varepsilon)V_{s,\text{tot}} = (1-\varepsilon)\left(A_{cs,s} \cdot dz\right) \tag{8}$$

where $V_{s,\text{tot}}$ is the total volume (includes the sorbent and voids), ε is the void fraction, and $A_{cs,s}$ is the cross-sectional area of the total volume. The total mass of the sorbent beads is determined by:

$$M_s = \rho_s V_s = \rho_s (1-\varepsilon)\left(A_{cs,s} \cdot dz\right) \tag{9}$$

where ρ_s is the density of the sorbent beads. The specific surface area of the packed microcapsules, a_s, inside the sorption bed is estimated by:

$$a_s = \frac{6}{d_{\text{caps}}}(1-\varepsilon) \tag{10}$$

where d_{caps} is the diameter of the microcapsules. The available heat and mass transfer area is calculated by:

$$A_{h,m} = a_s V_{\text{tot}} = \frac{6}{d_{\text{caps}}}(1-\varepsilon)\left(A_{cs,s} \cdot dz\right) \tag{11}$$

The overall heat U_h and mass U_m transfer coefficients (neglecting the heat and mass resistance of the thin air layer, see assumption 5 and Fig. 8**b**) are determined by:

$$U_h = \left[\frac{1}{h_{c,h}} + \frac{t_{\text{shell}}}{k_{\text{shell}}}\right]^{-1} \tag{12}$$

$$U_m = \left[\frac{1}{h_{c,m}} + \frac{t_{\text{shell}}}{D_{\text{wv,shell}}}\right]^{-1} \tag{13}$$

The terms $1/h_{c,h}$ and $1/h_{c,m}$ in Eqs. (12) and (13) are the convective heat and mass transfer resistances, respectively. The terms $t_{\text{shell}}/k_{\text{shell}}$ and $t_{\text{shell}}/D_{\text{wv,shell}}$ represent the conductive heat and mass transfer resistances through the shell material, respectively. In the above equations, t_{shell}, k_{shell}, and $D_{\text{wv,shell}}$ are the thickness, thermal conductivity, and moisture mass diffusivity of the shell.

The convective heat transfer coefficient $h_{c,h}$ was estimated using the derived expression for spherical particles:

$$h_{c,h} = \frac{\overline{Nu}_D \cdot k_{air}}{d_{\text{caps}}} = \frac{k_{air}}{d_{\text{caps}}}\left[2 + \frac{0.779}{(2/Re_D^{0.25}+1)} Re_D^{1/2} Pr^{1/3}\right] \tag{14}$$

Due to the analogy between the heat and mass transfer, the convective mass transfer coefficient,$h_{c,m}$, can be estimated by (see also assumption 6: for air, $Le_a \simeq 1$) [36]:

$$h_{c,m} = \frac{h_{c,h}}{\rho_a c_{p,a}} Le_a^{-2/3} = \frac{h_{c,h}}{\rho_a c_{p,a}} \tag{15}$$

The humidity content of the air at the sorbent-air interface, ω_s, can be calculated using the psychometric relations as follows [37]:

$$\omega_s = \frac{0.622 RH_s}{\frac{P}{P_{vs}} - RH_s} \tag{16}$$

$$P_{vs} = e^{(23.196 - 3816.44/(T_s - 46.13))} \tag{17}$$

where P is the atmospheric pressure, and P_{vs} is the water saturation vapor pressure. The corresponding relative humidity of air at the sorbent-air interface can be estimated using the experimental isotherm curves. The experimental isotherm curve of the microcapsules measured using a thermogravimetric vapor sorption analyzer (IGA-002, Hiden Isochema) is shown in Fig. 9. The data points were curve-fitted to find a polynomial that describes the relation between the relative humidity and water uptake, and is expressed as:

$$RH_s = 0.00198 - 0.0887X_s - 0.747X_s^2 + 9.07346X_s^3 - 12.45188X_s^4 + 4.97313X_s^5 \tag{18}$$

4. Results and discussion

4.1. Pressure drop across the sorption bed

The electric power consumption is directly related to the pressure drop across the bed. A high pressure drop is not favorable because it results in a high operating cost and high noise levels. For this reason, the variation of pressure drop across the sorption bed with respect to air inlet velocity presented was investigated and reported in Fig. 10. Considering the practical operating conditions, the maximum pressure drop (at 2 m/s) was 200 Pa/m. This value is two orders of magnitude lower than the reported values for simple packed beds (12,897 Pa/m) [38].

Temperature and humidity ratio profiles of the baseline test (Process air: T = 30 °C and RH = 60%) are reported in Fig. 11**a** and Fig. 11**b**,

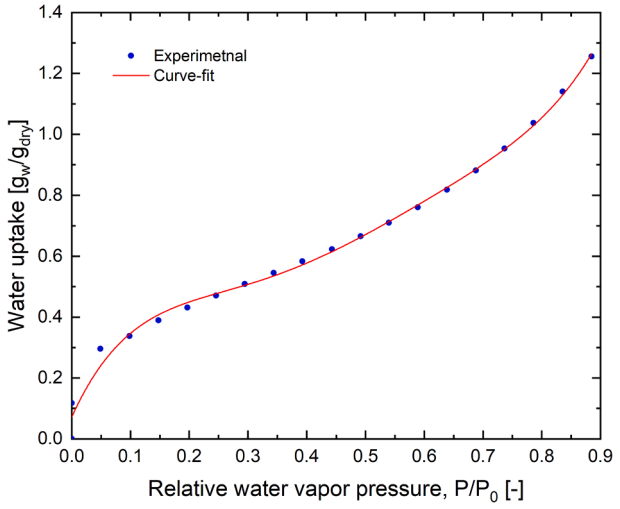

Fig. 9. The isotherm of the microcapsules: (a) experimental (thermogravimetric vapor sorption analyzer test); and (b) the proposed curve-fit, Eq. (18).

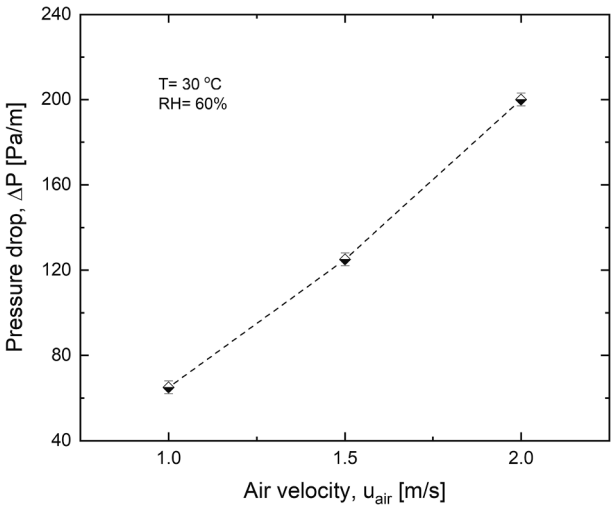

Fig. 10. The variation of pressure drop across the sorption bed with the air velocity.

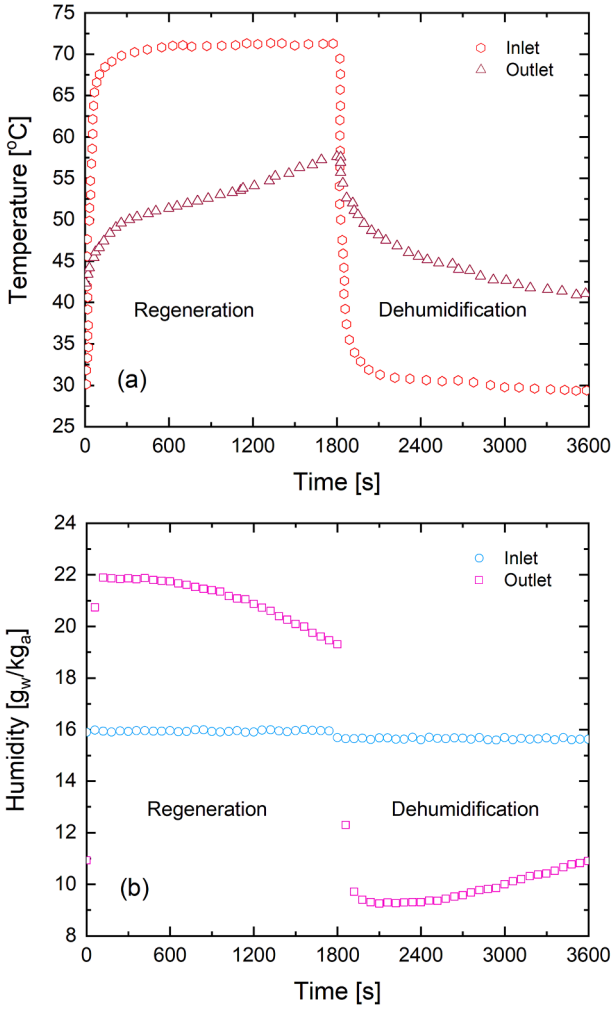

Fig. 11. (a) Temperature; and (b) humidity profiles during the regeneration ($T_{reg,i}$ = 60 °C and $RH_{reg,i}$ = 5%) and dehumidification processes ($T_{pro,i}$ = 30 °C and $RH_{pro,i}$ = 60%) in the base line experiment.

respectively. During the regeneration process (see Fig. 6), the heat is transferred from the hot and dry air to the microcapsules. As a result, the air exists from sorption bed relatively cooler, and water is released (from the microcapsules) to the air stream which results in an increase of its moisture content.

In the dehumidification process (see Fig. 6), the warm and humid process air cools down the bed, and the moisture is simultaneously absorbed by the liquid desiccant inside the microcapsules. At the beginning of the process, air dehumidification is less effective because the microcapsules are still hot from the regeneration process. Once the bed is adequately cooled, the dehumidification process reaches its maximum value and then it gradually decreases due to the increasing water content in the microcapsules.

4.2. *Effect of the process air inlet relative humidity*

The effect of supplied air inlet relative humidity on the moisture removal rate (MRR) is presented in Fig. 12**a**. As expected, the higher the relative humidity, the higher the driving force for the mass transfer from the humid air to the liquid desiccant inside the microcapsules, and consequently, the higher the moisture removal rate. As the relative humidity of the process air was increased from 50% to 70%, the moisture removal rate increased from 45 g/s m^3 to 53 g/s m^3 (+18%). The increase in the moisture content of the incoming air was also shown to

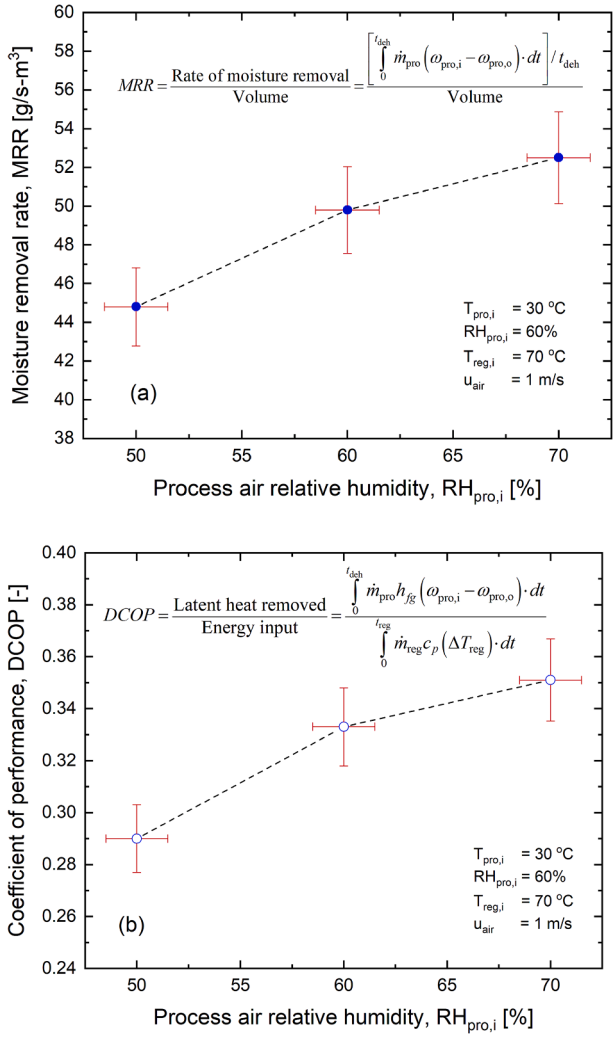

Fig. 12. The effect of process air inlet relative humidity on: (a) the moisture removal rate; and (b) the coefficient of performance ($T_{pro,i}$ = 30 °C, $T_{reg,i}$ = 70 °C, u_{air} = 1 m/s, and t_{deh} = t_{reg} = 30 min).

have a positive impact on the dehumidification coefficient of performance (DCOP) as presented in Fig. 12**b**. This is because the rate of moisture removal increases while the energy input remains the same, see Eq. (2). This means that the system would be more energy efficient in applications with higher relative humidity levels, e.g., greenhouses.

4.3. Effect of the process air inlet temperature

The results showed that warmer process air would result in a lower system capacity to remove the moisture as presented in Fig. 13. At the same relative humidity, as the inlet temperature of the process air was increased from 25 °C to 35 °C, the removal rate decreased by 12% (from 51 to 45 g/s-m^3). On the other hand, the coefficient of performance increased by 10% (from 0.30 to 0.33). This can be explained by the fact that in warmer environments less energy is required to heat the air to the regeneration temperature, and the increase in energy consumption outweighs the reduction in the moisture removal rate.

4.4. Effect of regeneration air temperature

The effect of regeneration temperature on the performance of the system is presented in Fig. 14. The results showed that the change in the moisture removal rate was directly proportional to the change in the regeneration temperature. Increasing the regeneration temperature

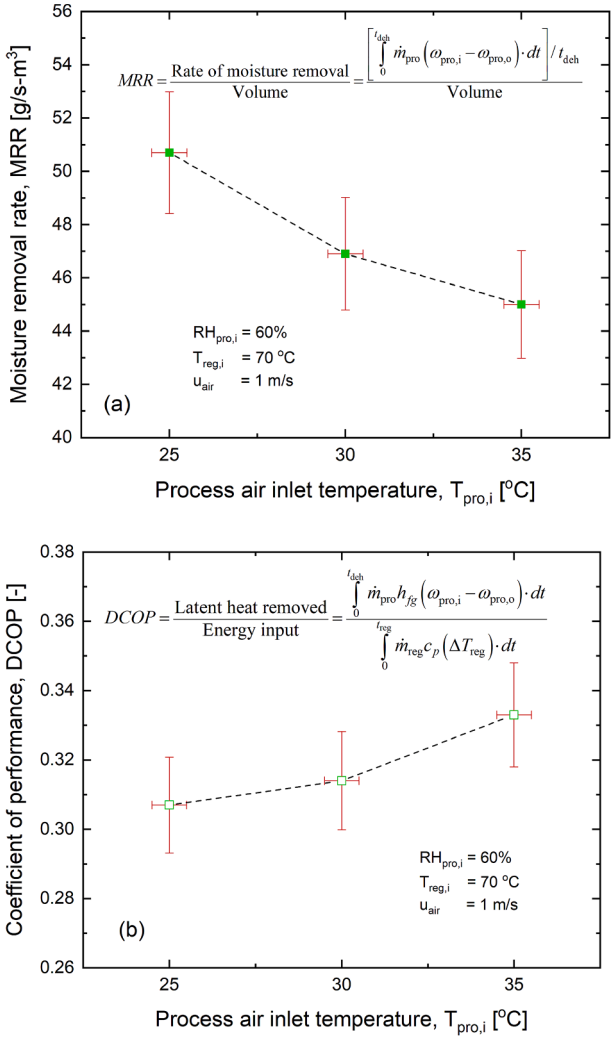

Fig. 13. The effect of process air inlet temperature on: (a) the moisture removal rate; and (b) the coefficient of performance ($RH_{pro,i}$ = 60%, $T_{reg,i}$ = 70 °C, u_{air} = 1 m/s, and t_{deh} = t_{reg} = 30 min).

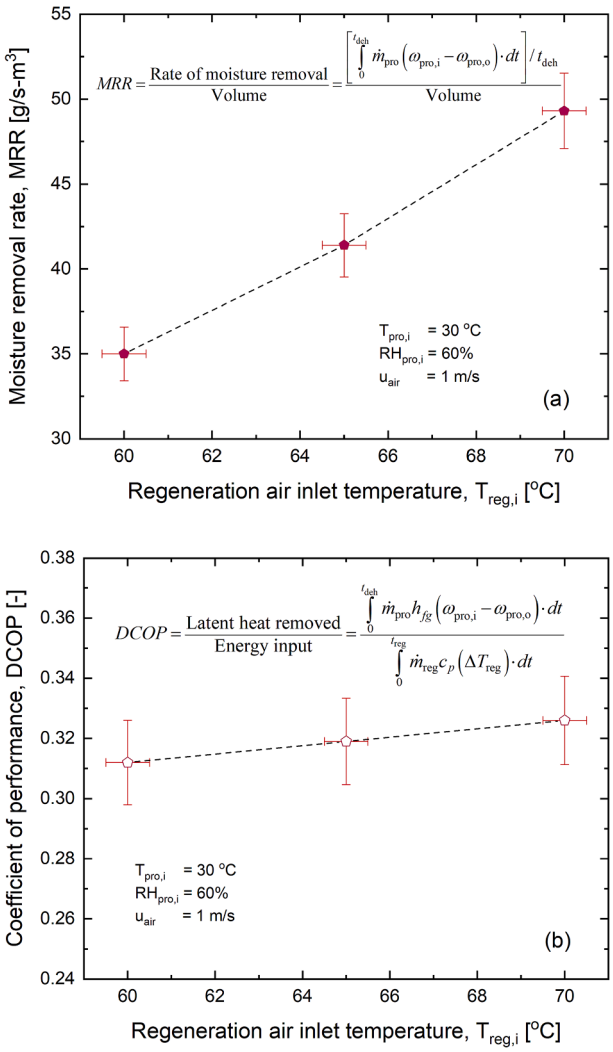

Fig. 14. The effect of regeneration air inlet temperature on: (a) moisture removal rate: and (b) the coefficient of performance ($T_{pro,i}$ = 30 °C, $RH_{pro,i}$ = 60%, u_{air} = 1 m/s, and t_{deh} = t_{reg} = 30 min).

from 60 °C to 70 °C resulted in a 43% increase in the moisture removal rate (see Fig. 14**a**). Higher regeneration temperatures resulted in higher supplied energy, which helps overcome the heat of absorption, which in turn, results in more water molecules to be desorbed from the liquid desiccant. Despite the increase in the energy input due to the increased regeneration temperature, the coefficient of performance remained almost constant, Fig. 14**b**. This indicates that the increase in the energy input can be compensated by the gain in the moisture removal rate (see Eq. (2)). Therefore, working with high regeneration temperatures will be favorable for a higher system performance.

4.5. Effect of air velocity

Increasing the air velocity (i.e., flow rate) from 1 to 2 m/s resulted in a 47% increase in the moisture removal rate as shown in Fig. 15**a**. This is due to the increase in the number of water molecules in the air stream available for absorption, in addition to the enhancement in the convective heat and mass transfer coefficients. However, the improvement in the rate of moisture removal was accompanied by a 29% drop in the coefficient of performance Fig. 15**b**. This was because the thermal energy requirement also increased as the flow rates were increased. The maximum moisture removal rate (at 2 m/s) was 75 g/s-m^3, i.e., a two-fold higher than that reported for LiBr conventional packed towers

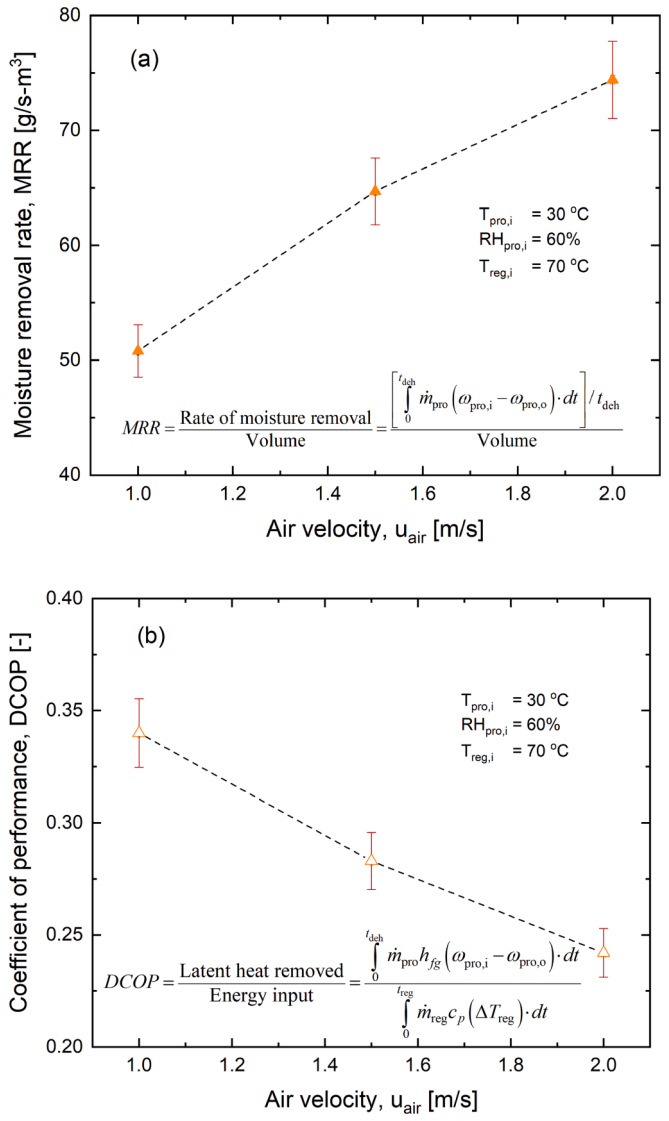

Fig. 15. The effect of air inlet velocity on: (a) the moisture removal rate; and (b) the coefficient of performance ($T_{pro,i}$ = 30 °C, $RH_{pro,i}$ = 60%, $T_{reg,i}$ = 70 °C, u_{air} = 1 m/s, and t_{deh} = t_{reg} = 30 min).

(35 g/s-m^3) that were tested under typical dehumidification working conditions (Process air: inlet temperature = 25–35 °C, and relative humidity = 60–70%) [14].

4.6. Model validation

The coupled energy and mass balance equations, Eqs. (4) to (7), were discretized along the sorption bed length using the finite element method, which resulted in a system of ordinary differential equations. A MATLAB code was written to solve the highly coupled heat and mass ordinary differential equations using the MATLAB ordinary differential equation solver [39]. The parameters used in the model validation are presented in Table 4. A comparison between the predicted temperature and humidity profiles and the experimental results for the baseline test are shown in Fig. 16**a** and Fig. 16**b**. The main deviations occur in the outlet air temperatures, as the model values are slightly higher than the measured ones. This might be attributed to the fact that the inlet temperatures were assumed to be constant in the model, whereas in real experiments, it takes few seconds for the inlet temperatures to reach the intended set values. The comparison between the predicted moisture removal rates and the coefficient of performance with the experimental data in terms of relative difference ((model - data)/model × 100) with various test conditions is presented in Fig. 17. The model was able predict all the experimental values with a ± 10% relative difference.

Table 4
The parameters used in the model validation.

Parameter	Value
Sorption bed length,L	180 mm
Channel height,H	1.5 mm
Microcapsules' outer diameter,d_{caps}	700 μm
Shell thickness,t_{shell}	70 μm
Thermal conductivity of the shell,k_{shell}	0.2 W/m-K
Water vapor mass diffusivity,$D_{wv,shell}$	3.7x10^{-6} m^2/s
Heat of absorption,ΔH_s	2,600 kJ/kg

4.7. Optimization study

A parametric study using the validated model revealed that the various design and operating conditions would have different impacts on the system performance. Therefore, there is a need to conduct an optimization study. Parameters that include design variables (sorption bed length, channel height) and the "controllable" operating conditions (air velocity and half-cycle time) were selected to maximize both the moisture removal rate (MRR) and the dehumidification coefficient of

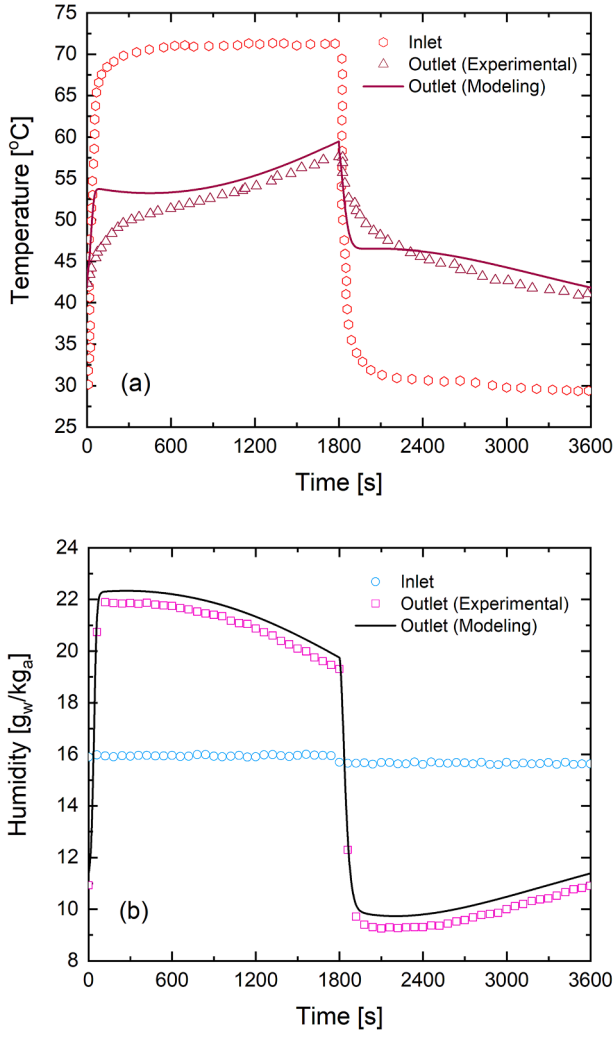

Fig. 16. Validation of the predicted (a) temperature; and (b) humidity profiles by the model with the experimental results of the baseline test ($T_{pro,i}$ = 30 °C, $RH_{pro,i}$ = 60%, $T_{reg,i}$ = 70 °C, u_{air} = 1 m/s, and t_{deh} = 30 min).

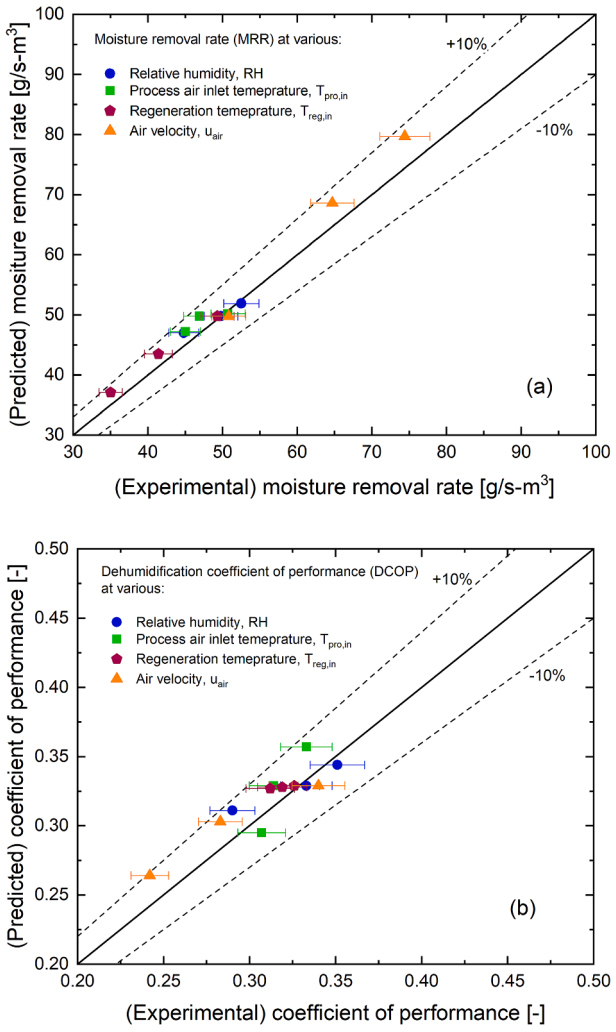

Fig. 17. Validation of the predicted (a) moisture removal rate; and (b) coefficient of performance by the model with the experimental results at the various test conditions.

performance (DCOP). The mathematical formulation of the multi-objective optimization problem is:

Minimize:

$$-MRR,\ -DCOP \tag{19}$$

Subject to:

$$\begin{aligned} &100\ \text{mm} \leqslant L \leqslant 300\ \text{mm} \\ &1.0\ \text{mm} \leqslant H \leqslant 3\ \text{mm} \\ &0.5\ \text{m/s} \leqslant u_{air} \leqslant 2\ \text{m/s} \\ &5\ \text{min} \leqslant \text{Half - cycle time} \leqslant 60\ \text{mins} \end{aligned} \tag{20}$$

The MATLAB code was linked to OASIS software [40], i.e., an optimization platform that is based on proprietary algorithms. OASIS algorithms integrate several approaches from metamodeling, machine learning, statistical analysis, and mathematical programming. The algorithms follow an iterative sampling, learning, resampling process that identifies the best solution in less time. More information about OASIS optimization algorithm can be found in Ref. [40]. The experimental results showed that high inlet temperatures and low relative humidity levels of the process air have adverse effects on the moisture removal rates (see Fig. 12 and Fig. 13). An optimization study was conducted to optimize the design for the worst-case scenario in an environment with the lowest relative humidity ($RH_{pro,i}$ = 50%) and the highest process inlet temperature ($T_{pro,i}$ = 35 °C) in the typical working range ($T_{pro,i}$ = 25–35 °C, $RH_{pro,i}$ = 50–70%).

The pareto front that shows all the efficient solutions for the multi-objective (the moisture removal rate and coefficient of performance) problem is presented in Fig. 18. One can observe that there is a trade-off between the maximum removal rate and the coefficient of performance values that can be balanced. By considering that liquid desiccant dehumidifier systems are often powered by a free-energy source, such as solar thermal energy or waste-heat, perhaps achieving the highest moisture removal rates should be prioritized. In cases where energy efficiency is of the same importance, other feasible solution(s) in the Pareto frontier that represent the best trade-off removal rate and coefficient of performance may be selected. The result from the optimization study shows that the absorber design can be optimized to realize removal rates value of ~ 130 g-s/m^3 with a coefficient of performance of 0.25, which is 270% higher than the highest value (35 g/s-m^3) reported for the conventional packed towers that use LiBr liquid desiccant [14]. The result of the optimization study is summarized in Table 5.

5. Conclusion

A novel liquid desiccant dehumidification system in which spherical micro-absorbers were used in a “packed-sheet” setup was designed and tested under the typical working conditions. The experimental results have shown the following:

- Both the moisture removal rate and the coefficient of performance will increase as the process air becomes more humid;
- In warmer environments, the moisture removal rate will decrease, but the coefficient of performance will be better because less thermal energy will be required to heat up the air to the required regeneration temperature;
- The change in the moisture removal rate is directly proportional to the change in the regeneration temperature. An increment of 10 °C in the regeneration temperature (from 60 °C to 70 °C, while maintaining a constant moisture content) resulted in a 40% increase in the moisture removal rate, while no noticeable change was observed in the coefficient of performance. Therefore, increasing the regeneration temperature in this range is favorable;
- Increasing the air velocity from 1 to 2 m/s resulted in a 47% increase in the moisture removal rate, at the expense of the coefficient of the performance dropping by 29%;
- The maximum moisture removal rate during the experiments was 75 g/s-m^3, i.e., a two-fold increase compared to the values reported for

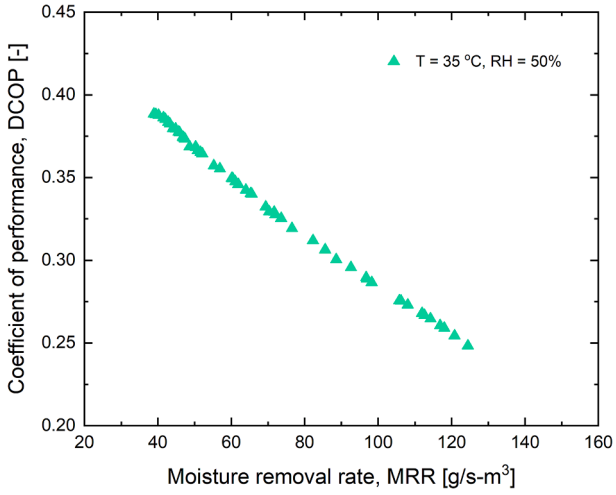

Fig. 18. The pareto front curve of the multi-objective (moisture removal rate and coefficient of performance) optimization.

Table 5
The optimal solution for (the moisture removal rate and the coefficient of performance) multi-objective optimization problem.

Optimal Parameter	Value
Sorption bed length,L	160 mm
Channel height,H	1.0 mm
Air velocity,u_{air}	2 m/s
Process (half-cycle) time,t_{deh}	15 min
Moisture removal rate,MRR	130 g/s-m^3
Dehumidification of performance,$DCOP$	0.25

the conventional LiBr gas–liquid absorption packed towers (35 g/s-m^3); and

An optimization study, using a validated mathematical model, indicated that the design variables and controllable operating conditions can be optimized to maximize the performance and achieve moisture removal rate values of up to 135 g/s-m^3 (270% higher than the conventional liquid desiccant systems) with a coefficient of performance of 0.25.

The presented system has the potential to eliminate the practical challenges associated with the conventional liquid desiccant dehumidification systems such as solution carryover, crystallization, and corrosion. The presented approach herein can be used to explore the possibility of producing micro-absorbers using other hygroscopic liquid desiccants such LiCl and $CaCl_2$ salt solutions. Utilizing the ionic liquids, which have higher sorption capacities than the salt solutions, in such micro-absorbers can significantly contribute to reducing the size and cost of the proposed liquid desiccant dehumidification system.

Declaration of Competing Interest

The authors declare that they have no known competing financial interests or personal relationships that could have appeared to influence the work reported in this paper.

Data availability

Data will be made available on request.

Acknowledgement

The authors gratefully acknowledge the financial support of the Natural Sciences and Engineering Research Council of Canada (NSERC) through the Advancing Climate Change Science in Canada Grant No. ACCPJ 536076-18, and NSERC Discovery Grant No. RGPIN-2022-04371.

References

[1] Agency IE. Energy Technology Perspectives 2017. 2017. https://doi.org/https://doi.org/https://doi.org/10.1787/energy_tech-2017-en.
[2] M.M. Rafique, P. Gandhidasan, H.M.S. Bahaidarah, Liquid desiccant materials and dehumidifiers – a review, Renew. Sustain. Energy Rev. 56 (2016) 179–195.
[3] B. Guieysse, C. Hort, V. Platel, R. Munoz, M. Ondarts, S. Revah, Biological treatment of indoor air for VOC removal: potential and challenges, Biotechnol. Adv. 26 (2008) 398–410.
[4] Farooq M, Wahid A, Kobayashi N, Fujita D, Basra SMA. Plant drought stress: effects, mechanisms and management. Sustain. Agric., Springer; 2009, p. 153–88.
[5] M.I. Nizovtsev, V.Y. Borodulin, V.N. Letushko, A.A. Zakharov, Analysis of the efficiency of air-to-air heat exchanger with a periodic change in the flow direction, Appl. Therm. Eng. 93 (2016) 113–121.
[6] J. Fernández-Seara, R. Diz, Uh'ia FJ, Dopazo A, Ferro JM., Experimental analysis of an air-to-air heat recovery unit for balanced ventilation systems in residential buildings, Energy Convers Manage 52 (2011) 635–640.
[7] J. Han, H. Guo, R. Brad, Z. Gao, D. Waterer, Dehumidification requirement for aGreenhouse located in a cold region, Appl. Eng. Agric. 31 (2015) 291–300.
[8] L.G. Gordeeva, G. Restuccia, A. Freni, Y.I. Aristov, Water sorption on composites "LiBr in a porous carbon", Fuel Process. Technol. 79 (2002) 225–231.
[9] C. Bales, P. Gantenbein, A. Hauer, H.-M. Henning, D. Jaenig, H. Kerskes, et al., Thermal properties of materials for thermo-chemical storage of solar heat, Rep B2-IEA SHC Task 2005;32.
[10] R. Qi, C. Dong, L.-Z. Zhang, A review of liquid desiccant air dehumidification: from system to material manipulations, Energ. Buildings 215 (2020), 109897.
[11] P. Bansal, S. Jain, C. Moon, Performance comparison of an adiabatic and an internally cooled structured packed-bed dehumidifier, Appl. Therm. Eng. 31 (2011) 14–19.
[12] S. Sehgal, J.L. Alvarado, I.G. Hassan, S.T. Kadam, A comprehensive review of recent developments in falling-film, spray, bubble and microchannel absorbers for absorption systems, Renew. Sustain. Energy Rev. 142 (2021), 110807.
[13] S. Jain, P.K. Bansal, Performance analysis of liquid desiccant dehumidification systems, Int. J. Refrig 30 (2007) 861–872.
[14] X.H. Liu, X.Q. Yi, Y. Jiang, Mass transfer performance comparison of two commonly used liquid desiccants: LiBr and LiCl aqueous solutions, Energy Convers Manag 52 (2011) 180–190.
[15] Y. Chen, X. Zhang, Y. Yin, Experimental and theoretical analysis of liquid desiccant dehumidification process based on an advanced hybrid air-conditioning system, Appl. Therm. Eng. 98 (2016) 387–399.
[16] R.M. Lazzarin, A. Gasparella, G.A. Longo, Chemical dehumidification by liquid desiccants: theory and experiment, Int. J. Refrig 22 (1999) 334–347.
[17] N. Fumo, D.Y. Goswami, Study of an aqueous lithium chloride desiccant system: air dehumidification and desiccant regeneration, Sol. Energy 72 (2002) 351–361.
[18] S. Jain, P.L. Dhar, S.C. Kaushik, Experimental studies on the dehumidifier and regenerator of a liquid desiccant cooling system, Appl. Therm. Eng. 20 (2000) 253–267.
[19] G.A. Longo, A. Gasparella, Experimental and theoretical analysis of heat and mass transfer in a packed column dehumidifier/regenerator with liquid desiccant, Int. J. Heat Mass Transf. 48 (2005) 5240–5254.
[20] L. Zhang, E. Hihara, F. Matsuoka, C. Dang, Experimental analysis of mass transfer in adiabatic structured packing dehumidifier/regenerator with liquid desiccant, Int. J. Heat Mass Transf. 53 (2010) 2856–2863.
[21] M.M. Bassuoni, An experimental study of structured packing dehumidifier/regenerator operating with liquid desiccant, Energy 36 (2011) 2628–2638.
[22] C.G. Moon, P.K. Bansal, S. Jain, New mass transfer performance data of a cross-flow liquid desiccant dehumidification system, Int. J. Refrig 32 (2009) 524–533.
[23] S. Jain, S. Tripathi, R.S. Das, Experimental performance of a liquid desiccant dehumidification system under tropical climates, Energy Convers Manag 52 (2011) 2461–2466.
[24] S.-M. Huang, M. Yang, X. Yang, Performance analysis of a quasi-counter flow parallel-plate membrane contactor used for liquid desiccant air dehumidification, Appl. Therm. Eng. 63 (2014) 323–332.
[25] D.G. Moghaddam, P. LePoudre, G. Ge, R.W. Besant, C.J. Simonson, Small-scale single-panel liquid-to-air membrane energy exchanger (LAMEE) test facility development, commissioning and evaluating the steady-state performance, Energ. Buildings 66 (2013) 424–436.
[26] H. Bai, J. Zhu, Z. Chen, L. Ma, R. Wang, T. Li, Performance testing of a cross-flow membrane-based liquid desiccant dehumidification system, Appl. Therm. Eng. 119 (2017) 119–131.
[27] Z. Chen, J. Zhu, H. Bai, Y. Yan, L. Zhang, Experimental study of a membrane-based dehumidification cooling system, Appl. Therm. Eng. 115 (2017) 1315–1321.
[28] M. Bhowmik, P. Muthukumar, R. Anandalakshmi, Experimental investigation on structured packed bed liquid desiccant dehumidifier: An optimal mixture design of experiments strategy, Int. J. Refrig 122 (2021) 232–244.
[29] T. Chen, Z. Dai, Y. Yin, X. Zhang, Experimental investigation on the mass transfer performance of a novel packing used for liquid desiccant systems, Sci Technol Built Environ 23 (2017) 46–59.
[30] L.S. Tan, A.M. Shariff, K.K. Lau, M.A. Bustam, Factors affecting CO2 absorption efficiency in packed column: A review, J. Ind. Eng. Chem. 18 (2012) 1874–1883.
[31] G.A. Longo, A. Gasparella, Experimental analysis on chemical dehumidification of air in a packed column by hygroscopic salt solution: Comparison between structured and random packings, HVAC&R Res 12 (2006) 713–729.
[32] S.J. Kline, Describing uncertainty in single sample experiments, Mech. Eng. 75 (1953) 3–8.
[33] R. Narayanan, W.Y. Saman, S.D. White, M. Goldsworthy, Comparative study of different desiccant wheel designs, Appl. Therm. Eng. 31 (2011) 1613–1620.
[34] S. De Antonellis, C.M. Joppolo, L. Molinaroli, Simulation, performance analysis and optimization of desiccant wheels, Energ. Buildings 42 (2010) 1386–1393.
[35] X.J. Zhang, Y.J. Dai, R.Z. Wang, A simulation study of heat and mass transfer in a honeycombed rotary desiccant dehumidifier, Appl. Therm. Eng. 23 (2003) 989–1003.
[36] T.L. Bergman, T.L. Bergman, F.P. Incropera, D.P. Dewitt, A.S. Lavine, Fundamentals of heat and mass transfer, John Wiley & Sons, 2011.
[37] M.J. Moran, H.N. Shapiro, D.D. Boettner, M.B. Bailey, Fundamentals of engineering thermodynamics, John Wiley & Sons, 2010.
[38] Y.-C. Chiang, C.-H. Chen, Y.-C. Chiang, S.-L. Chen, Circulating inclined fluidized beds with application for desiccant dehumidification systems, Appl. Energy 175 (2016) 199–211.
[39] MathWorks MATLAB software, https://www.mathworks.com 2020.
[40] OASIS optimization software, www.empowerops.com 2022.